PUBLISHED BY INSTITUTE OF PHYSICS PUBLISHING AND SISSA
RECEIVED: *July 3, 2008*
ACCEPTED: *August 22, 2008*
PUBLISHED: *September 8, 2008*

CMS silicon tracker alignment strategy with the Millepede II algorithm

G. Flucke,[a] P. Schleper,[a] G. Steinbrück[a] and M. Stoye[b]*

[a] *Institut für Experimentalphysik, Universität Hamburg, Germany*
[b] *Imperial College London, London, U.K.*
E-mail: markus.stoye@cern.ch

ABSTRACT: The positions of the silicon modules of the CMS tracker will be known to $O(100\ \mu\text{m})$ from survey measurements, mounting precision and the hardware alignment system. However, in order to fully exploit the capabilities of the tracker, these positions need to be known to a precision of a few μm. Only a track-based alignment procedure can reach this required precision. Such an alignment procedure is a major challenge given that about 50000 geometry constants need to be measured. Making use of the novel χ^2 minimization program Millepede II an alignment strategy has been developed in which all detector components are aligned simultaneously and all correlations between their position parameters taken into account. Different simulated data, such as Z^0 decays and muons originated in air showers were used for the study. Additionally information about the mechanical structure of the tracker, and initial position uncertainties have been used as input for the alignment procedure. A proof of concept of this alignment strategy is demonstrated using simulated data.

KEYWORDS: Detector alignment and calibration methods (lasers, sources, particle-beams); Analysis and statistical methods.

*Corresponding author

2008 JINST 3 P09002

Contents

2008 JINST 3 P09002

1. CMS tracker alignment challenge

A precise alignment of the silicon tracker of CMS [1, 2] is mandatory in order to fully exploit its physics capabilities. The tracker consists of 25644 silicon sensors which have altogether a surface of about 200 m^2. It is the largest silicon tracker ever built, having a diameter of 2.4 m and a length of 5.4 m. The silicon strip tracker is composed of several sub-detectors, namely the Tracker Inner Barrel (TIB), the Tracker Outer Barrel (TOB), the Tracker Inner Disks (TID), and the Tracker Endcaps (TEC). Single sided silicon strip modules consist of either one or two daisy-chained silicon sensors with custom read-out electronics. On selected positions, a second module is mounted back-to-back with a stereo angle of 100 mrad. The two modules combined are referred to as a stereo module and can provide a two-dimensional measurement. The pixel detector is divided into the Pixel Barrel (PB) and the Pixel Endcaps (PE). Figure 1 shows a schematic overview of one

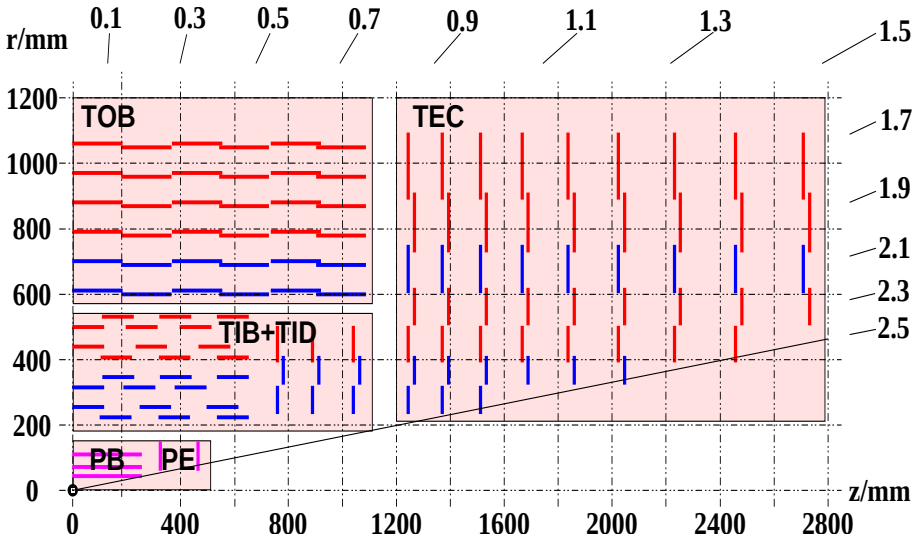

Figure 1. Layout of one quarter of silicon tracker in the r-z projection with η coverage indicated. Modules illustrated in blue are stereo modules.

quarter of the tracker in the r-z projection and the pseudo-rapidity coverage. Altogether there are 13300 modules.

The initial uncertainties on the module positions from the mounting precision, survey measurements, and the hardware alignment system [3] will be of the order of a few hundred microns. The effect of such a misalignment on the performance is expected to be significant. For example, the transverse momentum resolution in the central region decreases from about 1% to 5% for muons with a transverse momentum of 100 GeV. Only track-based alignment procedures will be able to improve on this initial situation. To avoid significant adverse effects due to misalignment, the positions of detectors should be known to the order of a few μm, which is an order of magnitude smaller than the typical intrinsic resolution of the modules. However, even small displacements can have an effect on track parameter measurements if the displacements are correlated.

The precision with which the tracker can be aligned is completely dependent on what data are available. This availability varies widely for different high energy physics experiments. Lepton colliders typically have a well defined centre-of-mass energy, with the centre-of-mass frame and the experimental frame being identical (e.g. LEP experiments) or at least the transformation between the frames is well known (e.g. b-factories). Muon pair production in such an environment is an ideal source of tracks for alignment, as the muons are exactly back-to-back and have a *known momentum* value. Such events can be used as a *standard reference* to calibrate the momentum measurement via the alignment procedure. Hadron colliders do not have access to such a good reference sample, making detector alignment much more complicated.

In order to achieve a fast turn around, the computing time for alignment should be of the order of hours and the memory required should not exceed few Gigabytes. Assigning three alignment parameters to each single strip module and four parameters to the stereo modules and to the pixel modules, about 50000 alignment parameters are needed for the entire tracker. This is an order of magnitude larger than any previous alignment problem in high energy physics.

An alignment strategy is laid out in the next section, followed by a detailed description of the

2008 JINST 3 P09002

alignment algorithm (section 2). Using this algorithm difficulties of finding a unique solution are discussed (section 3). In section 4 a full scale alignment study is shown, using muons of Z^0 decays and cosmic ray muons. The impact of utilizing different data and different options of the algorithm are also studied. Finally the effect of the remaining misalignment on the reconstruction quality is presented in section 5.

The aim of a track-based alignment procedure is to reduce the bias and uncertainty of the fitted track parameters and to minimize the χ^2 of the track fits by correcting the positions of the detector components. The minimization of the χ^2 is important to ensure track and vertex recognition, because the χ^2 of the track fit can be used to identify hits that make exceptionally large contributions to the χ^2 and hence are likely to be incorrectly associated to tracks. However, even with the χ^2 minimized and the pattern recognition working well, it is still possible to end up with biased measurements of track parameters due to misalignment. Correlated displacements of modules that introduce a track parameter bias, but do not change the mean χ^2, are clearly a major challenge. Given this situation, a sophisticated alignment strategy will be required.

The most important ingredients for alignment are the tracks used. In addition to tracks from proton-proton collisions, tracks of muons from proton beam halo and cosmic rays will be important because they pass through detector components that are otherwise unconnected by tracks. In addition, correlated misalignment can be reduced with the help of reconstructed particle decays such as $Z^0 \rightarrow \mu\mu$. Data of interest are therefore:

- Tracks from proton-proton collisions;
- Muon tracks originating from the proton beam halo or cosmic rays;

Other key ingredients are the known uncertainties on the module positions and the correlations between them, which are introduced by the mechanical support structures of the tracker. The information comes from:

- Mechanical mounting precision;
- Support structure layout;
- Survey measurement precision;
- Hardware alignment information;

However, the use of this initial knowledge requires a good understanding of the temperature dependence of the mechanical properties, and the possible time evolution of the module positions. Generally, the information extracted in situ from track data is preferred. In addition to the tracks χ^2, certain symmetries of the track parameter distributions can be used to extract additional information about the module positions. Some examples of this are:

- Identical transverse momenta spectra for both muons in $Z^0 \rightarrow \mu^-\mu^+$ decays;
- Independence of the transverse momentum distributions on the azimuthal angle ϕ;

To make optimal use of these pieces of information, an alignment algorithm must be able to fulfill the following requirements:

2008 JINST 3 P09002

- Inclusion of all correlations between position parameters;
- Incorporation of survey measurements;
- Fast turn around time and computational feasibility;

The algorithm used in this study is briefly described in the next section.

1.1 Alignment algorithms

Most track-based algorithms are based on the χ^2 minimization principle. In the CMS tracker a track typically consists of about 20 independent measurements such that the five parameters of a helix track are, in principle, overdetermined. These measurements, u_m, are compared to predictions from the track model. The predicted measurements, u_p, from the track model depend, for track j, on the vector of track parameters, τ_j, and the parameters, $\mathbf{p}$, that describe the position, orientation and deformation of the detectors. The normalized residual, z_{ij}, between the predicted hit position and the recorded measurement of hit i is given by:

$$z_{ij} = \frac{u_{ij;m} - u_{ij;p}(\tau_j, \mathbf{p})}{\sigma_{ij}}. \tag{1.1}$$

The uncertainties, σ_{ij}, for each module do not contain correlations between the hit measurements, which are, in any case, generally not significantly correlated. Exceptions occur only if measurements from different modules are combined into a single measurement (stereo modules) or if particle interactions with material are a major source of uncertainty, which is only the case for low momentum tracks. For the tracks used in this study these correlations can be neglected.

Requiring optimal agreement between the track model and the data means minimizing a function that depends on the normalized residuals. Most commonly the function

$$\chi^2(\tau, \mathbf{p}) = \sum_j \left(\sum_i z_{ij}^2(\tau_j, \mathbf{p}) \right) \tag{1.2}$$

is minimized with respect to all τ_j and $\mathbf{p}$. Generally, all overdetermined parameters from objects that are reconstructed in the tracker, like vertices for example, can be used for alignment.

2. Global linear χ^2 minimization with constraints

2.1 Linearization of normalized residuals

The first step in the χ^2 minimization is to linearize the minimization problem. This is equivalent to a linearization of the normalized residuals z_{ij} in the χ^2-function:

$$\chi^2 = \sum_j \left(\sum_i z_{ij}^2(\tau_j, \mathbf{p}) \right) \simeq \sum_j \left(\sum_i \frac{1}{\sigma_{ij}^2} \left(u_{ij;m} - u_{ij;p}(\tau_{j0}, \mathbf{p_0}) + \frac{\partial u_{ij;p}}{\partial \mathbf{p}} \mathbf{a} + \frac{\partial u_{ij;p}}{\partial \tau_j} \delta\tau_j \right)^2 \right), \tag{2.1}$$

where $\mathbf{p_0}$ are the initially-assumed geometry parameters and τ_{j0} are the initially-assumed track parameters. The derivatives are determined at $\mathbf{p_0}$ and τ_{j0}. The geometric correction parameters $\mathbf{a} = \delta\mathbf{p}$ are referred to as alignment parameters in the following. The alignment parameters are

2008 JINST 3 P09002

known as global parameters, as they are not specific to a single track or event. The parameter corrections for a track (or other reconstructed objects like a vertex) are specific to a single event and hence the parameters $\delta\tau_j$ are known as local parameters. The linearized minimization leads to a system of linear equations that needs to be solved [6]. The number of free parameters in these equations is given by the total number of local and global parameters. The number of local parameters can be of the order of millions. In addition, there are some 50000 global parameters. This leads to a symmetric square matrix with millions of rows.

2.2 Matrix reduction

Given the size of the matrix involved, its reduction is mandatory. A customized algorithm that makes use of the special nature of local parameters is able to fulfill this task. In case of track-based alignment individual tracks are independent of each other apart from the fact that they use a common geometry description of the tracker. This leads to a special structure of the (normal equation) matrix:

$$\left(\begin{array}{c|c|c|c} \sum \mathbf{C}_j & \dots & \mathbf{G}_j & \dots \\ \hline \vdots & \ddots & 0 & 0 \\ \hline \mathbf{G}_j^T & 0 & \mathbf{\Gamma}_j & 0 \\ \hline \vdots & 0 & 0 & \ddots \end{array}\right)\left(\begin{array}{c} \mathbf{a} \\ \hline \vdots \\ \hline \delta\tau_j \\ \hline \vdots \end{array}\right) = \left(\begin{array}{c} \sum \mathbf{b}_j \\ \hline \vdots \\ \hline \beta_j \\ \hline \vdots \end{array}\right), \tag{2.2}$$

where the elements are given by:

$$(\mathbf{\Gamma}_j)_{kl} = \sum_i \frac{\partial z_{ij}}{\partial \tau_{jk}} \frac{\partial z_{ij}}{\partial \tau_{jl}}\,,\ (\beta_j)_k = \sum_i \frac{\partial z_{ij}}{\partial \tau_{jk}} z_{ij}\,,\ (\mathbf{C}_j)_{kl} = \sum_i \frac{\partial z_{ij}}{\partial a_{jk}} \frac{\partial z_{ij}}{\partial a_{jl}}\,,$$

$$(\mathbf{b}_j)_k = \sum_i \frac{\partial z_{ij}}{\partial a_{jk}} z_{ij}\,, \text{ and } (\mathbf{G}_j)_{kl} = \sum_i \frac{\partial z_{ij}}{\partial a_{jk}} \frac{\partial z_{ij}}{\partial \tau_{jl}}$$

This structure can be exploited to reduce the matrix size. The sub-matrices $\mathbf{\Gamma}_j$ include only derivatives with respect to local parameters, while the sub-matrices $\mathbf{C}_j$ depend only on global parameters. The matrices $\mathbf{G}_j$ include both. Products of global derivatives and the normalized residuals appear in $\mathbf{b}$, and β_j consist of local derivatives and the normalized residuals. A matrix $\mathbf{C}'$ and a vector $\mathbf{b}'$ can be defined as follows:

$$\mathbf{C}' = \sum_j \mathbf{C}_j - \sum_j \mathbf{G}_j \mathbf{\Gamma}_j^{-1} \mathbf{G}_j^T \qquad \mathbf{b}' = \sum_j \mathbf{b}_j - \sum_j \mathbf{G}_j (\mathbf{\Gamma}_j^{-1} \beta_j) \tag{2.3}$$

This leads to a much smaller equation system, which only contains the global parameters, $\mathbf{a}$:

$$\left(\begin{array}{c} \mathbf{C}' \\ \\ \end{array}\right)\left(\begin{array}{c} \mathbf{a} \\ \\ \end{array}\right) = \left(\begin{array}{c} \mathbf{b}' \\ \\ \end{array}\right) \tag{2.4}$$

Using this matrix size reduction from several million parameters to only the number of global parameters without losing correlation and precision is the core idea behind the Millepede algorithm [4]. In the course of the matrix reduction, correction parameters, $\delta\tau_j$, for each track and for a given geometry are calculated:

$$\delta\tau_j = \mathbf{\Gamma}_j^{-1}\beta_j \tag{2.5}$$

This is essential in order to extract the χ^2 of the track fits for a given geometry.

2.3 Constraints

A set of linear equality constraints on the alignment parameters can be expressed by a matrix equation: $\mathbf{Aa} - \mathbf{m} = 0$. These constraints are applied via Lagrange Multipliers leading to the following matrix equation [6]:

$$\left(\begin{array}{c|c} \mathbf{C}' & \mathbf{A}^T \\ \hline \mathbf{A} & 0 \end{array}\right)\left(\begin{array}{c} \mathbf{a} \\ \hline \lambda \end{array}\right) = \left(\begin{array}{c} \mathbf{b}' \\ \hline \mathbf{m} \end{array}\right) \tag{2.6}$$

If Lagrange Multipliers are used the matrix is no longer positive definite, which has to be kept in mind when choosing methods to solve the equation system.

2.3.1 Support structure constraints

The CMS Tracker consists of a hierarchy of support structures as illustrated in figure 2. Each support structure can be given additional alignment parameters. If structures at different levels of the hierarchy are aligned at the same time, equality constraints need to be applied in order to avoid a singular matrix. For example, a translation of a support structure corresponds directly to translations of all its subcomponents. A common translation of the subcomponents could cancel this movement, so common translations of the subcomponents with respect to the support structure must be forbidden by applying equality constraints. The calculation of the derivatives of the rigid body alignment parameters of support structures and the calculation of the equality constraints can be found in [7].

2.4 Numerical stabilization

The minimization does not need to have a unique solution which leads to a bad condition of the matrix (close to singular) and hence eventually to numerical problems. For each alignment parameter, a presigma term $1/\sigma_p^2$ is added to the diagonal matrix entry of the parameter. This term slows down the change of the parameters per iteration and improves the stability of the solution (condition) of the matrix equation. Alignment corrections significantly larger than the corresponding presigma are allowed after several iterations. Optimal values of the presigmas of the alignment parameters of the modules were found to be a factor of ten smaller than the initial position uncertainties with respect to the next supporting structure [7]. The presigmas of support structures were set to their position uncertainties.

2008 JINST 3 P09002

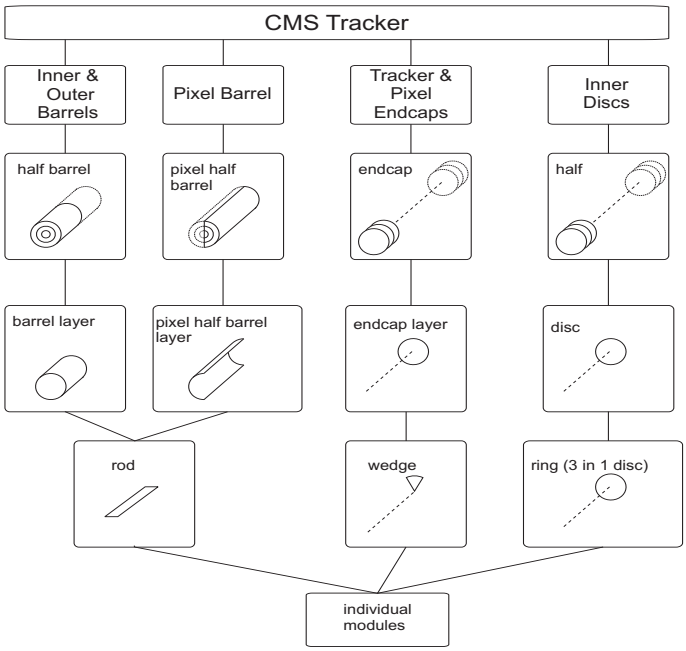

Figure 2. Illustration of the hierarchical support structures used for the alignment study. This software implementation of the support structures follows the physical support structures. However, small differences to the hardware structures do exist, e.g. the physical outer barrels do not have layers as support structures.

2.5 Linear equation solvers

The number of elements in the matrix $\mathbf{C}'$ in equation (2.4) is equal to the number of alignment parameters squared. In the case of the CMS tracker, there are about 50000 parameters, making a matrix inversion not feasible with the currently available computing power. However, there are algorithms that can solve linear equations much faster than by inversion, especially if the matrix is sparse (contains many zero elements). These algorithms do not modify the matrix whilst solving it. They require only the products of the matrix with vectors, which can be very fast for a sparse matrix. Several methods are implemented in Millepede II.

Inversion. The computing time needed for inverting a $n \times n$ matrix scales with n^3 and the memory needed to store the matrix scales with n^2. The inverted matrix is also the covariance matrix.

Diagonalization. Even more computing power is needed in order to diagonalize the matrix. However the eigenvectors and eigenvalues that are determined can be physically interpreted. Eigenvectors with small eigenvalues have little impact on the overall χ^2 and are therefore not well determined.

GMRES [8, 9]. If the matrix $\mathbf{C}'$ is sparse the memory demand can be reduced by storing only non-zero elements. The memory requirements are compared to other methods in table 1. If only tracks from the interaction point are used, the density (fraction of non-zero elements), q, of the matrix is about 1%. Since tracks from cosmic ray muons cross silicon modules which are not connected by a single track from the interaction point, these cosmic muon tracks do increase the

2008 JINST 3 P09002

Table 1. Memory requirements for the matrix $\mathbf{C}'$: n is number of global parameters, m the band width for the Choleskey band method and q the matrix density. The space needed for equality constraints is not included.

methods	memory space required [8 byte words]
inversion	n+n(n-1)/2
diagonalization	$n+n(n-1)/2+n^2$
band Cholesky	nm
GMRES (sparse)	n+qn(n-1)3/4

matrix density. If tracks are refitted with a common vertex, and cosmic muons and beam halo muons are used, the matrix density easily exceeds 10%.

Variable-Band Cholesky. Cholesky decomposition [10] can be used to solve a system of linear equations that can be represented by a symmetric matrix. If the matrix is a symmetric band matrix, this method is very fast. Only the matrix elements within the band need to be stored which requires only a small amount of memory. However, the matrix that is built in the course of the χ^2 minimization is not a band matrix. Ignoring the elements outside the chosen band means ignoring some correlations between alignment parameters. Hence, the solution obtained via the band Cholesky is an approximate solution. The variability of the band size allows the inclusion of equality constraints. The constraints are implemented via the matrix **A** as shown in equation (2.6). The variable bandwidth is set such that the full matrix **A** is included. The variable-band Cholesky method is used for preconditioning of the GMRES method.

2.6 Outlier rejection

In the χ^2-minimization procedure, the influence of a normalized residual increases linearly with its absolute value. Recorded hits that are many standard deviations away from the expected hit position (outliers) therefore have a large impact on the result. The minimization of the χ^2-function is only optimal if the uncertainties are Gaussian. Due to misassigned hits or non-Gaussian hit reconstruction errors, this assumption is not valid. For the outlier rejection mechanism, iterations will be required in order to achieve optimal performance. In Millepede, two outlier rejection methods have been developed. The first one is a track rejection while in the second hits are down-weighted.

In the former, when performing the matrix reduction within Millipede, the χ^2 and the number of degrees of freedom (ndof) for the track fit in each iteration are determined (equation (2.5)). A cut on the χ^2/ndof is applied to reject badly reconstructed tracks. However, in the first iteration the χ^2 is generally large, since the modules are misaligned and therefore only loose cuts can be applied. The cuts are then tightened with each iteration, since the χ^2 decreases with the improved alignment precision. However, the χ^2/ndof values of corrupted tracks remain large; hence they are rejected.

In the other outlier rejection mechanism, the impact of outlier hits is reduced by down-weighting their influence in the minimization procedure. A standard method (M-estimates) is not to minimize

2008 JINST 3 P09002

Table 2. Influence function and weight factor function derived from different outlier rejection functions and the χ^2 function.

function $f(z)$	influence(z)=$\frac{df}{dz}$	weight factor(z)=$\frac{df}{dz}\frac{1}{z}$
$\chi^2 \rightarrow \frac{z^2}{2}$	z	1
Huber $\rightarrow \begin{cases} \frac{z^2}{2} & \text{if} \lvert z\rvert < \mathrm{C_H} \\ C_H(\lvert z\rvert - \frac{C_H}{2}) & \text{if} \lvert z\rvert > \mathrm{C_H} \end{cases}$	z C_H	1 $\frac{C_H}{\lvert z\rvert}$
Cauchy $\rightarrow \frac{C_C^2}{2}\ln(1+(\frac{z}{C_C})^2)$	$z/(1+(\frac{z}{C_C})^2)$	$1/(1+(\frac{z}{C_C})^2)$

the χ^2-function but a different function F of the normalized residuals:

$$F(\tau, \mathbf{a}) = \sum_j \Big(\sum_i f(z_{ij}(\tau_\mathbf{j}, \mathbf{a})) \Big)$$

where f can be the Huber function or the Cauchy function (see table 2). If the Huber function is used the influence of normalized residuals that are larger than a parameter C_H, remains constant. A standard value for C_H is 1.345, which would result in an increase of the alignment uncertainty of 5%, if the error distributions are Gaussian. If the Cauchy function is used the influence decreases even for very large normalized residuals. The influence $\frac{df}{dz}$ and weight $\frac{df}{dz}\frac{1}{z}$ of a hit in the fit procedure for these functions are shown in figures 3 and 4, respectively.

In the studies presented in this article, the track fit (equation (2.5)) is done 5 times when using the down-weighting method, since the new weights lead also to new track parameters. The Huber-function is used as intermediate step for fast and controlled convergence towards the track parameters consistent with the Cauchy-function, which has the smallest weights for outliers. For the first two iterations the Huber-function is used, afterwards the Cauchy-function.

A small average weight of the hits from a track indicates that a number of hits are incorrectly measured. Hence, it is reasonable to reject these tracks.

2.7 Computational layout

An important aspect of alignment is the time needed for the analysis. It is therefore important that the information used by Millepede is collected in an efficient way. Collecting the necessary derivatives and measurements from the data can be parallelized. Therefore Millepede II is split into two parts, one part (Mille) produces binary files of the data needed for the alignment procedure. This part was interfaced to the CMS software. The other part (Pede) determines the alignment parameter from the binary files and is a standalone FORTRAN program. The separation between the CMS software and Pede makes it possible to use Pede easily in other experiments as well. The output of Pede are the alignment parameters used later on for reprocessing.

3. χ^2 invariant deformations

The diagonalization method of Millepede II has been used to identify the χ^2 invariant deformations described in section 1. The final alignment parameters $\mathbf{a}$ in terms of the normalized eigenvectors, $\mathbf{e}_k$,

2008 JINST 3 P09002

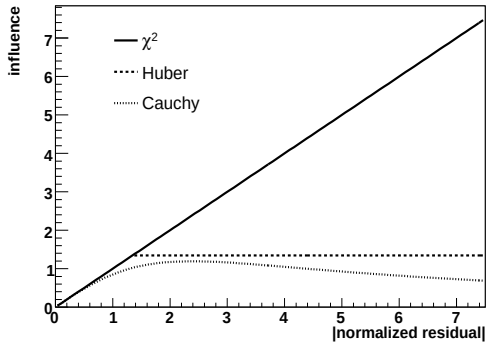

Figure 3. Influence functions for χ^2, Huber, and Cauchy methods.

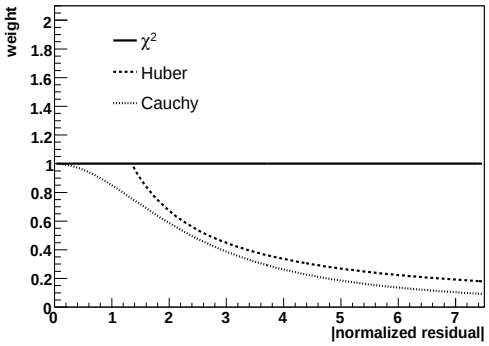

Figure 4. Weight factor functions for χ^2, Huber, and Cauchy methods.

Table 3. Alignment parameters used for strings, rods and ladders in the study of χ^2 invariant deformations.

type	number	alignment parameters	corresponding global coordinates
rods/strings	1340	u, v (if stereo), w, γ	$r\phi$, z (if stereo), r, rot$_r$
ladders	90	u, v, w, γ	$r\phi$, z, r, rot$_r$

are given by:

$$\sum_k \alpha_k \mathbf{e}_k = \mathbf{a}. \tag{3.1}$$

The eigenvectors with the smallest eigenvalues are the least well determined, since the eigenvalue is given by $1/\sqrt{\sigma_k}$, where σ_k is the uncertainty on the amplitude α_k of the eigenvector $\mathbf{e}_k$. The deformations corresponding to eigenvectors with the smallest eigenvalues were applied to the geometry in order to visualize the deformations. The diagonalization method is CPU intensive and hence the number of alignment parameters is limited to $O(10000)$. The alignment parameters and the dataset used to identify these deformations are described below.

Alignment parameters. In order to limit the computing requirements to an acceptable level, the smallest support structures, rather than the individual modules, were used in the barrel region for the study of deformations. These are the strings, rods (for the TIB and TOB) and ladders (for the PB) consisting of 3, 6, or 8 individual modules along the z (beam) direction, respectively. The alignment parameters per string, rod or ladder are the three translations u, v, w and the rotation, γ, around the normal of the support structure, all of which are illustrated in figure 5. For structures that consist only of single-sided strip modules, the insensitive direction along the strips (v) is neglected. The parameters are summarized in table 3. The χ^2 invariant deformations are independent from the initial misalignment, hence misalignment is not simulated.

2008 JINST 3 P09002

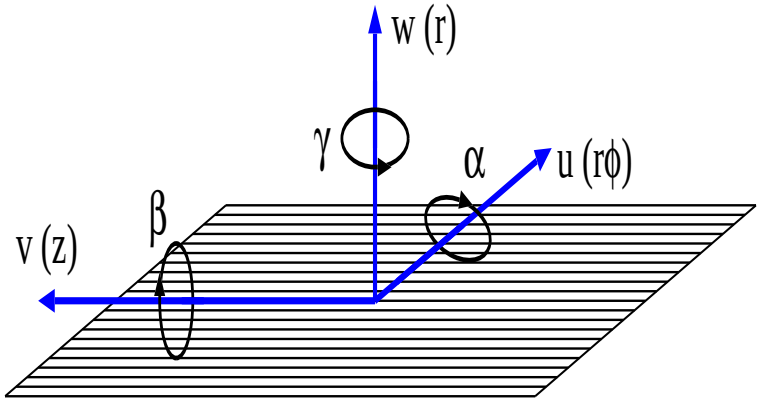

Figure 5. Schematic illustration of the alignment parameters. In brackets $(r, z, r\phi)$ are corresponding directions in the global CMS coordinate system in case of TOB modules.

Used track samples and selection. The $Z^0 \to \mu\mu$ events are of large importance for track based alignment because the high momentum of the muons and the relatively large muon mass lead to very small amounts of multiple scattering. In addition, pattern recognition and particle identification are relatively straight-forward for these isolated high momentum muons. The dataset used contains one million simulated Drell-Yan $Z^0/\gamma^* \to \mu\mu$ events produced with a pileup expected for nominal luminosity ($\mathscr{L} = 2 \times 10^{33}\text{cm}^{-2}\text{s}^{-1}$). The dataset was generated with Pythia [11], which is interfaced to the CMS software. The invariant mass of the muon pair is required to be at least 80 GeV. Each track is required to have at least 8 hits (stereo hits count twice) within the barrel region and a transverse momentum of more than 15 GeV. All measurements from detectors which are not included in this down-sized alignment study (endcap modules) are ignored.

Results. A set of basic χ^2-invariant deformations has been identified by studying the eigenvectors with the ten smallest eigenvalues. An example of the visualization of a badly-determined eigenvector deformation is shown in figures 6 and 7. They show an oscillation of the displacements in the radial direction r and in the tangential direction $r\phi$ as a function of the azimuthal angle ϕ. Functions of the form:

$$\Delta r(\phi) \sim \cos(n\phi + \omega) \quad \Delta r\phi(\phi) \sim \sin(n\phi + \omega) \quad \Delta z(\phi) \sim \cos(n\phi + \omega) \tag{3.2}$$

were fitted to the data in figure 7. Here ω is a constant shift and n is an integer mode number. Each mode n occurs twice, once with a constant shift $\omega = \omega_0$ and once with a shift $\omega = \omega_0 + 90^\circ/n$.

Mode 0 would be equivalent to a tracker expansion. This was the only mode found to impact the χ^2 value significantly, since the overall scale is fixed by the well known strip-pitch distances. Generally an expansion in r between different layers is accompanied by compression in $r\phi$ within these layers in order to keep the χ^2 of track fits small [7].

Another category of basic χ^2-invariant deformations are bending and shearing. Their average displacement in the r-ϕ direction can be described as a function of the radius of the modules:

$$\langle \Delta r\phi \rangle(r) \simeq p_0 + p_1 r + p_2 r^2 \quad \langle \Delta z \rangle(r) = z_0 + z_1 r \tag{3.3}$$

2008 JINST 3 P09002

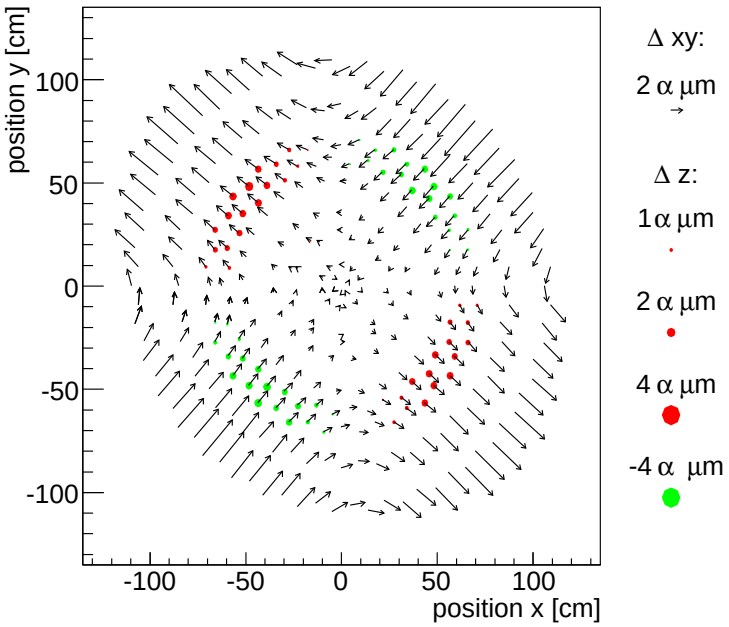

Figure 6. Illustration of the eigenvector of r-$r\phi$ mode 2 (see text). The radii of the circles represent the displacements in the z coordinate for the 2D detectors only. The colors decode the sign of the z displacements. The arrows indicate the displacements in the $r\phi$-plane. The amplitude α is the badly-determined parameter (equation (3.1)).

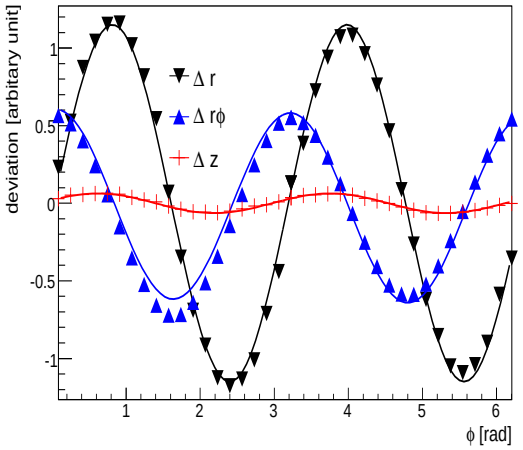

Figure 7. Displacements in $r, r\phi$, and z of rod positions in the fifth layer as a function of ϕ. The displacements correspond to a χ^2-invariant eigenvector. An r-$r\phi$ oscillation of mode 2 (equation 3.2) is fitted to the displacements.

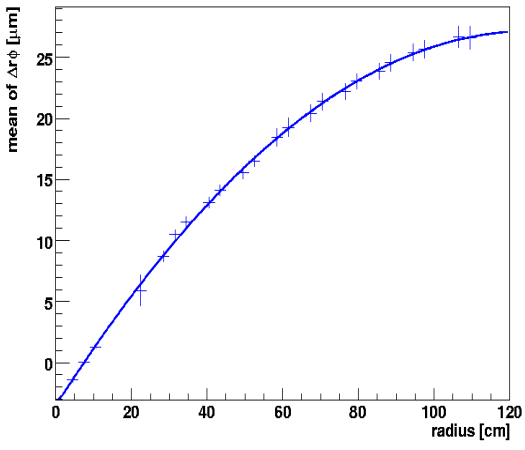

Figure 8. Fit of bending deformation function (equation (3.3)) to a χ^2-invariant deformation.

If the parameter p_2 is non zero, this is especially worrying, since it directly affects the curvature measurement. The fit, shown in figure 8, of equation (3.3) to the data clearly illustrates that this function approximates well the χ^2-invariant deformation. The bending and shearing deformation can vary along the *z*-axis, leading to a twist of the tracker. A summary of the basic deformations which were observed is illustrated in figure 9. The observed deformations are likely to remain after the alignment procedures and it is therefore important to understand their effect and find means to reduce their impact. More detailed studies on the deformations can be found in [7]. The use of datasets like cosmic muons and constraints like the vertex constraint for particles from the same interaction point are essential to fulfill this task, as will be seen in the following sections.

4. Full tracker alignment case studies

In this section alignment studies using all strip and pixel modules in both barrel and endcap are presented.

The *first data* scenario, as described in [12], is used as initial misalignment. This misalignment scenario is the one that is meant to represent approximately the initial position uncertainties before collisions for the silicon strip tracker. The correlated nature of displacements due to common support structures of modules is taken into account. The pixel modules are assumed to be aligned to about 15 μm in this scenario. The initial position uncertainties are shown in table 4.

In the alignment procedure the full tracker is aligned, i.e. all of the pixel and strip detector of barrel and endcaps. The module alignment parameters are defined with respect to center of the half barrels or the endcaps, respectively. The initial position uncertainty of rods is similar to the module position uncertainty and since rods only consist of a small number of modules this level was skipped. The layer levels are also skipped. The layers do not exist as support structure in the outer barrel and are also generally not misaligned in the *first data* scenario. Each object is given four alignment parameters: the translation parameters *u*, *v*, *w*, and the rotation parameter γ. The parameter *v* is skipped for single-sided strip modules. Altogether this amounts to 44432 alignment parameters.

The innermost 24 modules of each pixel endcap are not aligned since no track, which passes the selection criteria, passed them. However, the survey measurements of these modules with respect to well aligned neighboring modules is precise to the μm level and could be used to improve their position estimate. Furthermore, the track quality in this very forward region is not dominated by misalignment. The Z^0 sample described in the previous section is used. Half a million events are used with a vertex constraint, forcing the two muon tracks to a common vertex. In addition the Z^0 mass and width (approximated by a Gaussian) is used as input to the fit. A detailed description of this procedure can be found in [14]. Single muons, without any vertex or mass constraints, from 1.5 million Z^0 events were used to mimic 3 million $W\rightarrow \mu\nu$ events. These data roughly correspond to an integrated luminosity of 0.5 fb^{-1} of data taking. In addition a dataset of 25000 simulated cosmic ray muons with a momentum of at least 50 GeV was used. All the cosmic ray muons traverse the central barrel region. The pattern recognition was assumed to work perfectly for tracks from cosmic muons, in order to avoid additional uncertainties from a pattern recognition that has not yet been fully developed. Details of the simulation of cosmic muons can be found in [7]. All cosmic ray tracks were required to consist of at least 18 hits (stereo hits count twice) and have an initial

2008 JINST 3 P09002

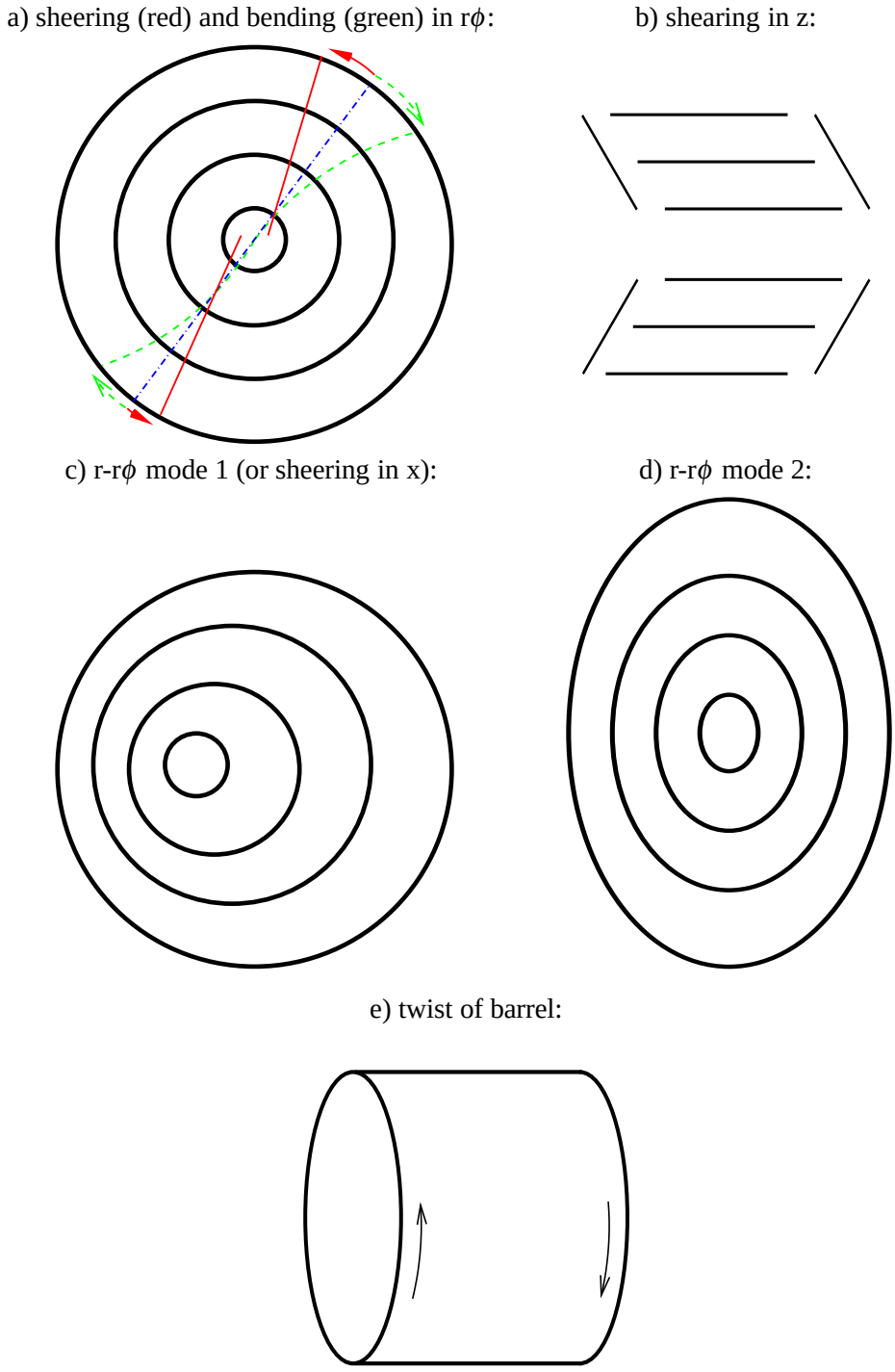

Figure 9. Schematic illustration of the χ^2 invariant deformations.

χ^2/ndof value below 10. Cosmic ray tracks with less than 18 hits tend to have many hits with small angles between the flight direction and the sensitive direction of the sensors (u), which leads to less reliable hit reconstruction and larger material effects.

2008 JINST 3 P09002

Table 4. Initial uncertainties according to the *first data* scenario [12], as used for the alignment procedure. A * denotes uncertainties that are assumed for alignment, but are zero in the simulation of the *first data* misalignment scenario. The presigmas applied for larger support structures are identical to their initial uncertainty, while the presigmas of the modules († rows) are a factor of ten smaller than their initial uncertainties. Note that rods, ladders, and petals have been misaligned, but are not introduced as alignment objects in this study.

type	Δ u [μm]	Δ v [μm]	Δ w [μm]	$\Delta\gamma$ [μrad]
PB half barrels	10	10	10	10
TIB half barrels	105	105	500	90
TOB half barrels	67	67	500	59
PE endcap	5	5	5	5
TID layers	400	400	400	100
TEC endcap	57	57	500	46
TPB modules†	13	13	13	10*
TIB modules†	200	200	200	10*
TOB modules†	100	100	100	10*
TPE modules†	2.5	2.5	2.5	10*
TID modules†	105	105	105	10*
TEC modules†	20	20	20	10*

The applied presigmas (section 2.4) for the alignment parameters of the modules are chosen to be a factor of 10 smaller than the initial uncertainties in the misalignment scenario. The presigmas for parameters of higher level structures are set to exactly equal the misalignment uncertainties. The applied presigmas are summarized in table 4.

The coordinate system is defined by the constraint that the sum of the alignment parameter vectors of the pixel half barrels has to be zero. Hence the average position of the pixel modules defines the origin of the coordinate system. In order to solve such a large alignment problem, the GMRES (see section 2) method in Millepede II is used. The linear equation system is preconditioned using the result of the band Cholesky method with a bandwidth of 6. Outlier hit down-weighting is used and tracks with an average weight of hits below 80% are rejected. The refit of tracks (local fit) is done with 5 iterations, since outlier down-weighting is applied. The number of the iterations for alignment parameter iterations (global fit) is also set to 5.

4.1 Alignment results

The alignment results are presented for the *first data* misalignment scenario, which was used as the starting point for the alignment procedure. The results are compared to the *long term* scenario. The *long term* misalignment scenario was an estimate used in the CMS Physics Technical Design Report (PTDR) [13], of the achievable alignment precision after reaching about 1 fb^{-1} of integrated

2008 JINST 3 P09002

luminosity. However, the results of the study do not include uncertainties from systematic effects like uncertainties on the magnetic field for example.

Figure 10 shows the remaining displacements after alignment for the barrel and endcap modules. The calculated positions in the best measured direction (rϕ) for the barrel (strip and pixel) modules have an uncertainty of only about 10 μm. For the endcap (strip and pixel) modules, the mean of the position residuals in rϕ after the alignment procedure is around 5 μm and with a spread of 23 μm. Barrel modules are better aligned since endcaps modules only indirectly profit from the use of cosmic tracks, which are vital for high precision (see next section), and very forwards tracks suffer from large material interaction effects and a small number of hits.

For the pixel modules the difference between true and estimated positions is presented in figure 11. The remaining position uncertainty in rϕ for the pixel barrel modules of 1 μm after alignment is an order of magnitude smaller than the *long term* estimate. The pixel module position uncertainties are of the order of a few μm for all directions and module types. The barrel module positions are generally better determined than those of the endcap modules.

The residuals between the true and estimated position in rϕ have been studied separately for the different detector components TIB, TID, TOB, and TEC (figure 11). Note that the double peak structure for the TOB modules is explained in the following paragraph. The position estimates improve with decreasing distance of the modules from the pixel detector. The intrinsic resolution of the modules closer to the beam line is generally better by construction and the number of hits larger. Furthermore, the displacements due to global deformation increase with distance from the pixel detector, whose modules define the origin of the coordinate system.

The overall remaining misalignment is dominated by a global χ^2 invariant deformation, that is, an r-$r\phi$ oscillation of mode one, with the maximum of r displacement at ϕ close to 90° (figure 12). A typical cosmic ray muon trajectory, which crosses the detector close to vertical, is also shown. It can be seen that the deformation displaces the modules in a direction almost parallel to a typical cosmic track, hence the hit measurements on the modules are not strongly influenced by this deformation. Figure 13 shows a similar oscillation with its maximal amplitude in a different direction. In this case a typical cosmic track would be kinked and hence this mode is suppressed by the use of cosmic muons. The studies performed here have shown that this is indeed the case.

The remaining oscillation is clearly visible in the displacements in $r\phi$-direction of the last layer of the barrel modules (figure 14). Figure 15 shows the average displacements in y as a function of the radius of the module position. A linear function $\langle \Delta y \rangle (r)$ would be expected for the displacement illustrated in figure 12 and, as can be seen in figure 14, this is indeed the case. This oscillation also explains the double peak like structure in the residual distribution for the outer barrel modules (figure 11, d). The peak at about 15 μm is caused by modules with a ϕ position around 0, while the peak at -15 μm is due to the modules with a ϕ position around $\pm\pi$.

2008 JINST 3 P09002

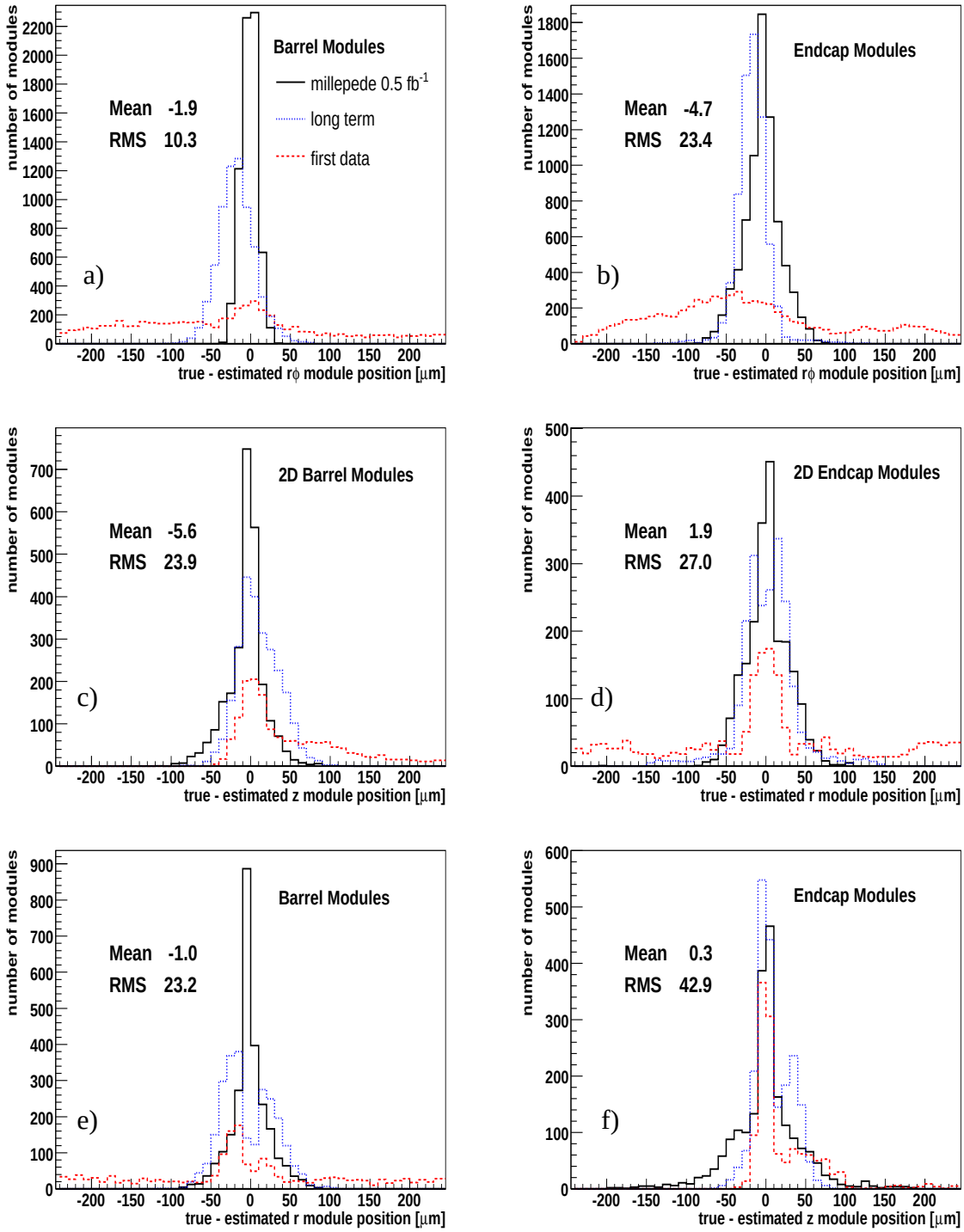

Figure 10. Residuals between true and estimated module positions in different directions and separately for barrel (left) and endcap (right) modules for the *first data* scenario, the *long term* scenario, and the result of the alignment procedure. The first row (a,b) shows the displacements in the $r\phi$ coordinate, the second row (c,d) the displacements in the other measured direction for stereo modules, and the third row the displacements in the direction normal to the module surface.

2008 JINST 3 P09002

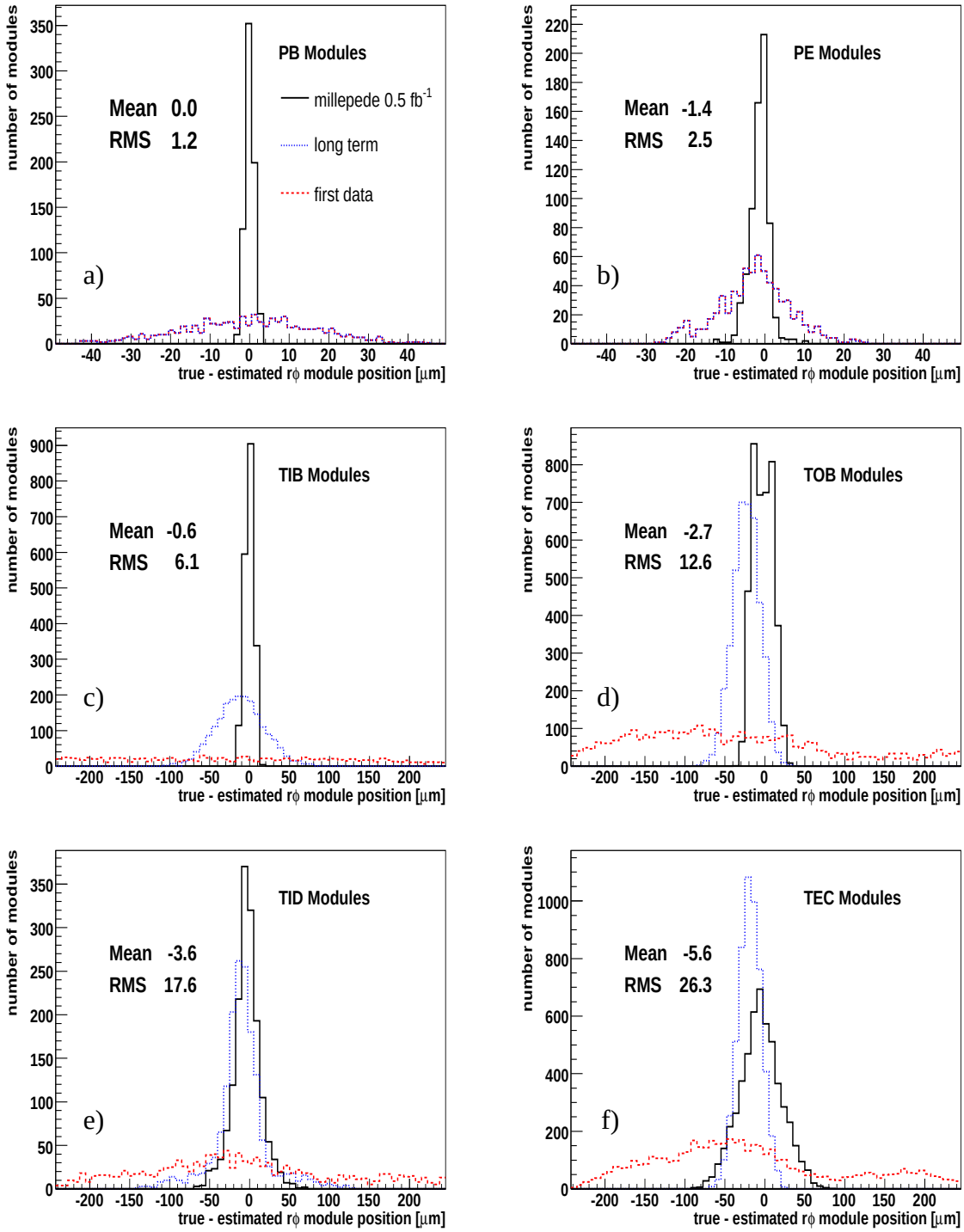

Figure 11. Residuals between true and estimated module positions in rϕ direction separated for the barrel detectors PB, TIB, TOB (left) and the endcap detectors PE, TID, TEC (right) modules for the *first data* scenario, the *long term* scenario, and after the alignment procedure. The misalignment of the pixel modules are the same for the *long term* and the *first data* scenarios, which is a feature of the scenarios.

2008 JINST 3 P09002

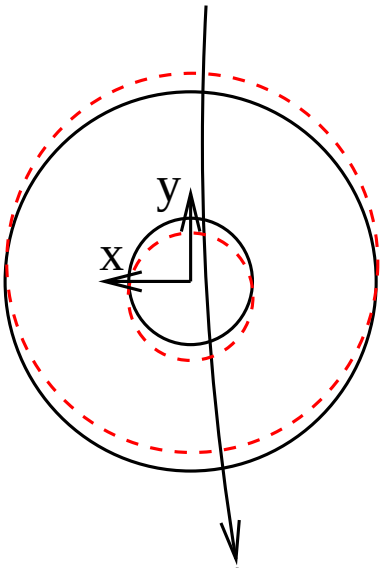

Figure 12. r-rϕ mode with a maximum amplitude of the r oscillation in the direction of y. The dashed lines illustrated the displaced geometry. In addition a typical cosmic trajectory is illustrated.

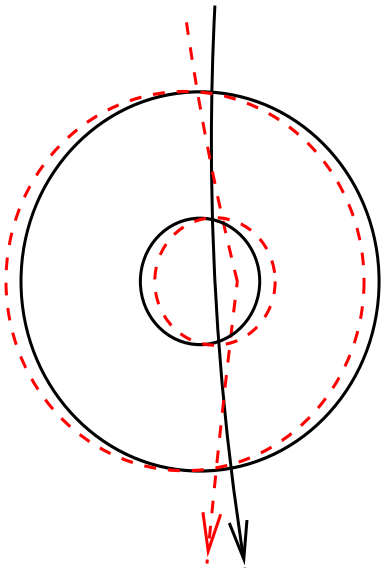

Figure 13. r-rϕ mode with a maximum amplitude of the r oscillation in the direction of x. The dashed lines illustrated the displaced geometry. In addition a typical cosmic trajectory is illustrated. The dashed trajectory illustrates the effect of the misalignment on the reconstructed track.

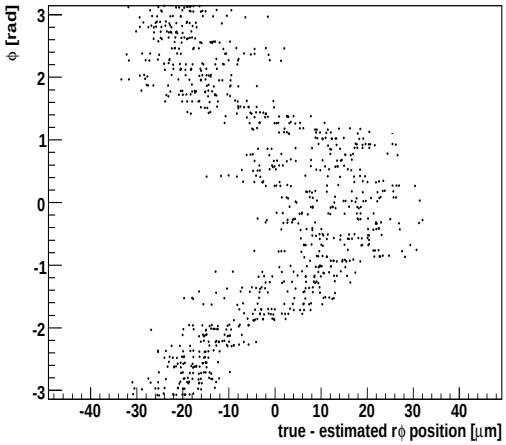

Figure 14. The displacements in rϕ of the barrel modules of the last layer versus ϕ after alignment.

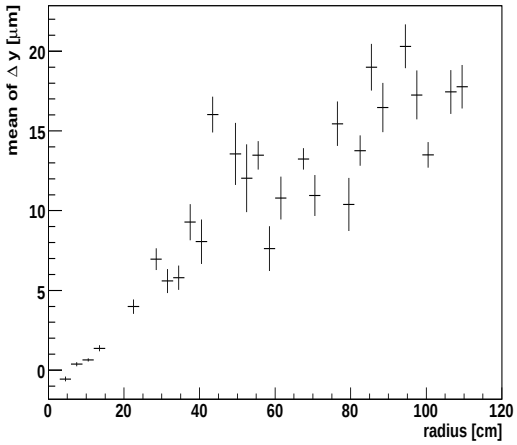

Figure 15. The r-rϕ mode 1 oscillation is visible as roughly linearly increasing mean displacement Δy as a function of the radius of the module position. The Δy of all modules are used in the plot.

2008 JINST 3 P09002

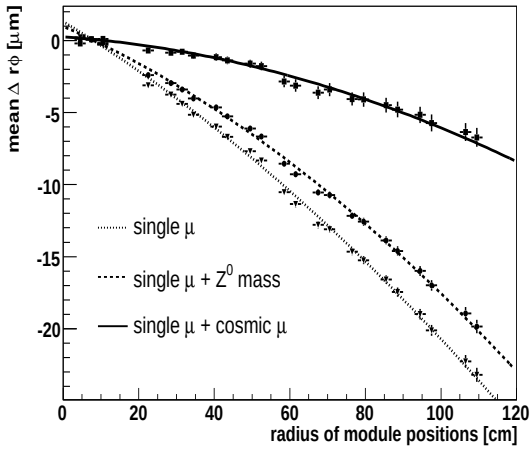

Figure 16. The mean of the displacements of barrel modules in rϕ as a function of the radius. The bending function (equation (3.3)) is fitted to the data points.

Computing requirements. The datasets in this study give a matrix density of 8.6% which translates to less than 2 Gigabyte of memory. The computing time used on a 64 Bit CPU is 1.2 hours.

When low energy cosmic rays are included, the alignment result does not significantly improve but the additional data lead to a higher matrix density (15%) because of the larger variation in the direction of flight. The computing time needed in this case increases to two hours. The building of the matrix takes about 50 minutes, whilst the solving of the matrix equation takes about 10 minutes, but is done five times in the course of the outlier rejection procedure.

It can therefore be concluded that the computing requirements are reasonable and can accommodate additional alignment parameters and datasets without problem.

4.2 Impact of different track sources

The datasets used for the alignment procedure were varied in order to study their impact. Three different dataset combinations were considered:

- Single muons from two million $Z^0 \rightarrow \mu\mu$ events;
- Single muons from 1.5 million $Z^0 \rightarrow \mu\mu$ events and half a million mass- and vertex-constrained Z^0 events;
- Single muons from two million $Z^0 \rightarrow \mu\mu$ events and 25000 high energy cosmic muons;

As an example the effects of the datasets on the shearing and bending deformations, which bias the curvature, vertex, and ϕ measurements, are presented. Figure 16 shows the average displacement of modules in the rϕ direction as a function of the module radius. As expected for bending and shearing deformations the function (equation (3.3)) fitted through the average displacements has a nonzero slope (shearing) and curvature (bending). The results are worst when the alignment is done with single muons from the Z^0 decays only. Adding mass-constrained Z^0s only slightly improves the results. The curvature bias from the bending deformation has the opposite effect

2008 JINST 3 P09002

on the momentum measurements for the two differently charged muons. Hence the effect due to the reconstructed Z^0 mass is small. Adding cosmic muons to the tracks from the interaction point however, significantly improves the results. The upper and lower sections of the tracker are directly connected via the cosmic muon track. Hence the momentum and ϕ measurement in the upper and lower part must match. This is only the case if the shearing and bending deformations are small. The cosmic muons appear to be important also for the reduction of other degrees of freedom in the minimization. More details can be found in [7].

4.3 Variation of statistics and event weights

The results for the 0.5 fb^{-1} scenario are very promising, but correspond to several months of data taking. Tests were also performed to understand what happens if important datasets like the cosmic muons are given more weight in the χ^2 minimization by using the same tracks multiple times. Five different dataset combinations were tested:

- Single muons from two million Z^0 events and 5000 high energy cosmic muon events;
- Single muons from two million $\text{Z}^0 \rightarrow \mu\mu$ events plus the full high energy cosmic muon dataset (25000 events);
- Single muons from one million Z^0 events and the full high energy cosmic muon dataset;
- Single muons from half a million Z^0 events and the full high energy cosmic muon dataset;
- Single muons from two million Z^0 events and using the full high energy cosmic muon dataset five times;

The results for the different datasets are summarized in table 5.

If high energy muons from cosmic rays are used the result is significantly improved, as demonstrated in section 4.2. Reducing the size of the cosmic ray dataset by a factor of five has a significant impact on the results. The means on the position errors after the alignment procedure in rϕ are reduced by the use of cosmics. The displacements in the other directions however, are not significantly affected by the reduced cosmic muon statistics.

If the number of single tracks from the interaction vertex is reduced by a factor of four, the precision of the module positions along the $r\phi$ coordinate is only slightly degraded. The modules measure the hit positions along the $r\phi$ direction very precisely (5-40 μm) and on average each module has thousands of hits even if only 0.5 million $\text{Z}^0 \rightarrow \mu\mu$ events are used. This means that the position would be determined to a fraction of a μm, if the global correlations of the alignment parameters were to be small. Clearly, the remaining displacements in rϕ are dominated by global deformations, and adding more tracks from the interaction point with similar energy will not improve things further. However, displacements along directions that are not so precisely measured by the module will profit more from higher statistics. The strategy of reweighting cosmic events by reusing the tracks five times only leads to slight improvements in some directions and slight degradations in others.

2008 JINST 3 P09002

Table 5. The mean and RMS values for the positions of the barrel (strip and pixel) and endcap (strip and pixel) modules in $r\phi$, r and z for different dataset combinations. In the case of the Z^0 events, no mass or vertex constraints were applied.

Z^0 (single μ) [millions]	events	2	2	1	0.5	2
cosmic μ [thousands]	events	5	25	25	25	5×25
barrel $r\phi$ [μm]	mean	-7.3	-3.2	-2.2	-1.4	-2.6
	rms	9.0	8.6	8.7	9.3	8.1
barrel z [μm]	mean	-4.5	-6.9	-9.8	-11.9	-9.9
	rms	24.2	24.6	28.9	33.2	25.2
barrel r [μm]	mean	0.0	0.0	0.2	1.2	0.0
	rms	23.5	23.1	25.6	32.3	22.7
endcap $r\phi$ [μm]	mean	-9.6	-6.1	-4.9	-4.1	0.8
	rms	22.6	22.5	24.7	26.8	22.3
endcap r [μm]	mean	1.2	1.5	1.2	1.2	1.6
	rms	26.0	25.5	28.4	32.3	25.0
endcap z [μm]	mean	-10.9	13.4	-17.8	-24.5	-16.6
	rms	52.6	51.9	53.2	52.2	51.8

4.4 Impact of outlier rejection

To test the impact of different outlier rejection methods (section 2.6), the scenario corresponding to an integrated luminosity of 0.5 fb^{-1} (as in section 4.1) has been used.

By default the hit down-weighting method is used to treat outliers in this study. Tracks with an average hit weight below 80% are rejected. The method of rejecting tracks if the standard deviation of the track fit are large has also been tested. The cuts placed on the number of standard deviation are 54, 27, 3, 3, and 3 for the five iterations. The alignment precision achieved is similar to that reached with the default hit down-weighting method. As a further test, the number of iterations was increased from 5 to 10.

In table 6 the alignment precisions achieved are compared. The comparison clearly demonstrates that outlier rejection is essential. For example, the position uncertainty for barrel modules along the rϕ direction is reduced from 18 μm to 10 μm by the use of outlier rejection. The exact number of iterations as well as the choice of the outlier rejection method has little impact on the results.

5. Alignment effects

The alignment results have so far been presented by comparing the true geometry parameters to the parameters found by the alignment procedure. However, the most interesting question is how the alignment affects the track parameter measurements. In order to study this the detector is misaligned according to the results of the alignment study using the 0.5 fb^{-1} datasets. The tracks which are most affected are muons with large transverse momentum. The relative error of the transverse

Table 6. The mean and RMS values of the positions of the barrel (strip and pixel) and endcap (strip and pixel) modules in the $r\phi$, r and z directions. The results from different outlier rejection procedures are shown.

outlier rejection method		none	down-weighting	χ^2 cut	down-weighting
iterations		1	5	5	10
barrel $r\phi$ [μm]	mean	1.9	-1.9	1.1	-4.3
	rms	17.9	10.3	9.6	8.4
barrel z [μm]	mean	-10.9	-5.9	-7.0	-3.3
	rms	33.7	23.9	23.6	20.9
barrel r [μm]	mean	-0.8	-1.0	-0.9	-1.0
	rms	32.7	23.2	22.8	20.5
endcaps $r\phi$ [μm]	mean	-3.1	-4.7	-1.3	-6.9
	rms	31.47	23.4	23.0	19.9
endcaps r [μm]	mean	1.7	1.9	1.6	1.9
	rms	35.9	27.0	26.3	23.7
endcaps z [μm]	mean	-6.0	0.3	-0.2	2.1
	rms	44.9	42.9	42.7	40.6

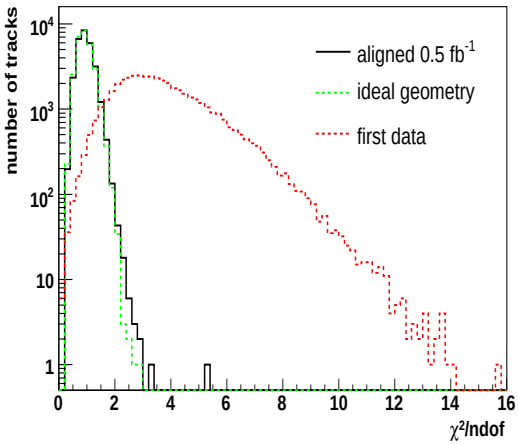

Figure 17. χ^2/ndof of track fits of 100 GeV muon tracks.

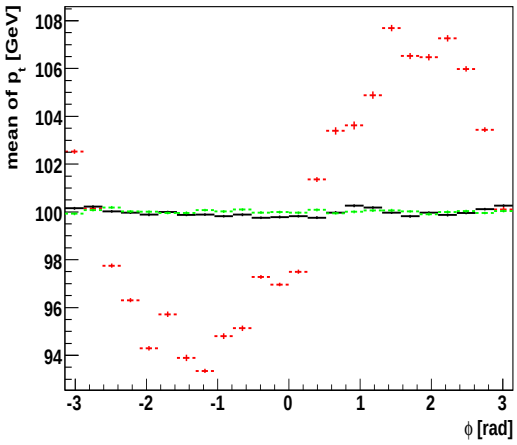

Figure 18. Mean of the reconstructed transverse momentum of 100 GeV muon tracks as a function of the azimuthal angle ϕ.

momentum measurement due to a bending deformation will for example increase linearly with the transverse momentum. Hence 50000 single μ^+ tracks from a single track simulator with a transverse momentum of exactly 100 GeV have been produced. The tracks are equally distributed in ϕ and η and their vertex position is set to (0,0,0). Material interaction effects are not taken into account and a homogeneous magnetic field is assumed for the simulation of these events.

The χ^2/ndof of the track fits is shown in figure 17. The average χ^2 values with the ideal

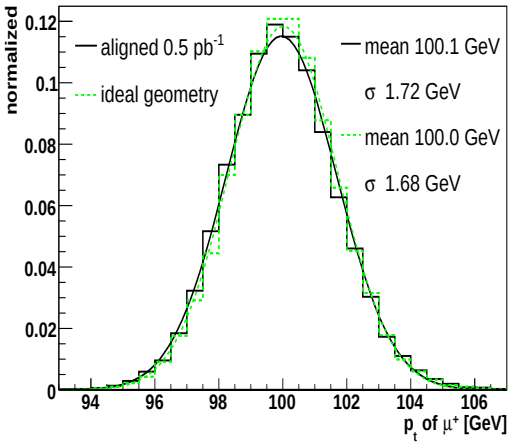

Figure 19. Reconstructed transverse momentum distributions of 100 GeV muon tracks fitted by Gaussian distribution.

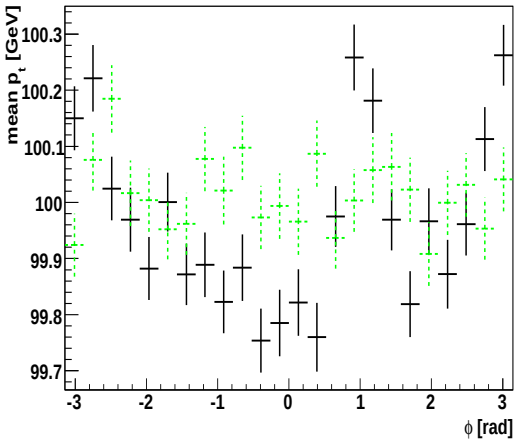

Figure 20. Average reconstructed transverse momentum of 100 GeV muon tracks as a function of ϕ.

geometry and after the alignment are very similar. The χ^2 values with the initial misalignment are clearly much larger. The bias on the transverse momentum is illustrated in figure 18. The initial biases are clearly almost completely removed. The reconstructed transverse momentum for all tracks is shown in figure 19. The relative error of the transverse momentum measurement at 100 GeV increases from (1.68 $\pm$ 0.008)% to (1.72 $\pm$ 0.008)% (statistical uncertainty) if the aligned geometry is used instead of the ideal geometry. A bias in the transverse momentum of (0.1 $\pm$ 0.01)% is introduced. The bias of the measured transverse momentum as a function of ϕ can be seen in figure 20, for both the aligned and the ideal geometry. A very small dependence on ϕ after alignment can be seen. The impact of the remaining misalignment on the reconstruction of the point of closest approach to the beam line is shown in figures 21 and 22. A bias of only about 1 μm in the measurement in the y coordinate is visible. The RMS of the distribution is about 7 μm both with and without misalignment. Also the degradation of the measured z position of the impact point is minimal. A bias of less than 2 μm is introduced. These small biases will hardly affect physics measurements.

6. Conclusions

The alignment of the CMS silicon tracking detector is a unique challenge compared to previous detectors. Sensor position uncertainties of a few μm, starting from $O(100)$ μm uncertainties, are required to fully exploit the physics potential of the tracker. In addition, the size of the tracker, with 13300 modules, is such that its alignment will be a major computational challenge, as alignment parameters for all modules need to be determined, many of which are highly correlated. The desired precision can only be achieved via track-based alignment. However, certain deformation of the tracker geometry can introduce a bias in the track parameter measurements, but leave the mean χ^2

2008 JINST 3 P09002

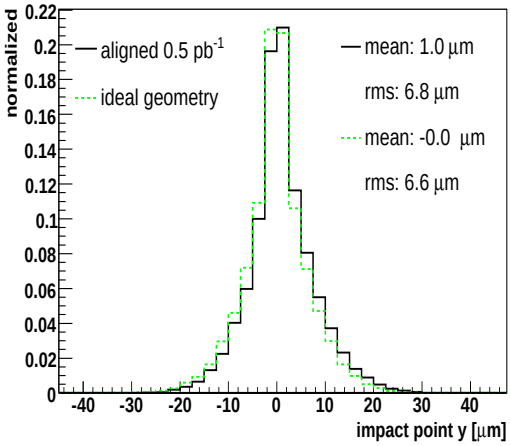

Figure 21. *y*-coordinate of the reconstructed impact point from 100 GeV muon tracks with a true impact point at zero.

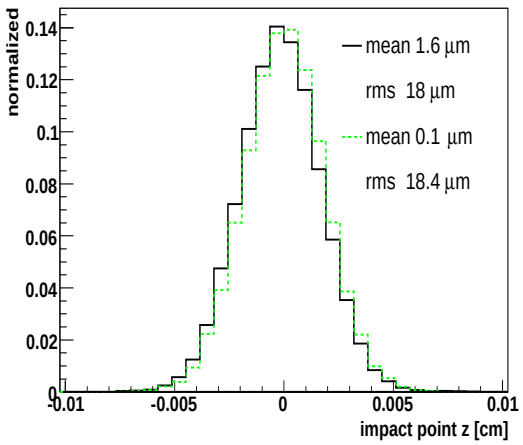

Figure 22. *z*-coordinate of the reconstructed impact point from 100 GeV muon tracks with a true impact point at zero.

of track fits unchanged. Given these issues, a sophisticated alignment strategy for the tracker must be developed. The alignment algorithm chosen to achieve this was Millepede II [5]. It is a non-iterative algorithm for solving χ^2 minimization problems incorporating all correlations between the geometry parameters. It is capable of dealing with the large number of position parameters (~ 50000) at CMS as well as constraints.

All possible degrees of freedom, i.e. those that can be determined by a χ^2 minimization using tracks as well as those that are χ^2 invariant, have been systematically studied. The χ^2 invariant deformations have been determined and classified. An alignment strategy is proposed which incorporates complementary sources of information which had been available as simulated data. A key ingredient in the alignment of the tracker is the use of complementary datasets like those from pp interactions at the central vertex, and cosmic ray muons, which connect different tracker parts via tracks. Vertex- and mass-constrained $Z^0 \rightarrow \mu\mu$ decays also increase the sensitivity to otherwise χ^2-invariant deformations. Position information gained during the mechanical mounting procedure and from survey measurements have also been implemented in the alignment procedure. The correlated nature of the initial displacements of the modules (with respect to the global coordinate system) arising from the displacement of large mechanical support structures, is exploited. A hierarchical structure of alignment parameters has been introduced, which reflects the mechanical support frames.

All these ingredients were used for a full scale alignment study, aligning all modules of the CMS silicon tracker in a single procedure. A *first data* misalignment scenario, aiming to represent the displacements at startup, has been used as the starting point. Samples of events with muons from Z^0 decays and single muons corresponding to an integrated luminosity of $0.5\,\text{fb}^{-1}$ were used, along with a sample of simulated cosmic ray muons. The module positions have been determined with an uncertainty of the order of 10 μm to 25 μm for the silicon strip modules in the

2008 JINST 3 P09002

well-measured $r\phi$ direction of the modules. For the pixel detector, a precision of a few μm was achieved. For tracks with transverse momentum of 100 GeV the bias on the transverse momentum measurement is reduced from around 7% to 0.2% at most after alignment. The transverse momentum resolution is degraded by less than 0.5% with respect to the ideal geometry. After alignment the change in the vertex position resolution is negligible and the vertex is systematically shifted by only one μm. Overall, the tracker is well aligned and the impact on physics measurements is very small. The CPU-time of the actual position parameter calculation was found to be only $\sim$2h and 2 GB of memory were required. This is remarkable, since the incorporation of all correlations is a computationally challenging task and only algorithms neglecting some or all correlations (in order to save CPU time and memory) had been proposed so far.

Studies were also performed to understand the importance of various elements of this alignment procedure. The datasets used were varied. It was found that cosmic muons are very important because they reduce a deformation (bending), which directly impacts the curvature measurement. The use of mass- and vertex-constrained Z^0 events also improved results, however they must be used in conjunction with other datasets to reduce all types of deformation to an acceptable level. This can be understood by the fact that some deformations do not strongly affect the mass measurement. A bias on the curvature measurement, for example, leads to opposite effects on transverse momentum measurement for the differently charged muons. Furthermore, the width of the Z^0 is large in comparison to the resolution. The impact of dataset size was also studied. This mimics condition before 0.5 fb^{-1} of integrated luminosity is reached. It is shown that the number of cosmic muons is very important, whilst the number of single tracks from the interaction point is less important, if the alignment precision along the well-measured $r\phi$ direction is regarded as the most relevant quantity. A further crucial issue in achieving successful alignment is the treatment of badly measured or incorrectly assigned hits. Studies showed that outlier rejection is vital. This is especially interesting, as this effect can already be observed in simulated data. Given that real data is likely to include even more outliers, it is clear that a good outlier rejection procedure must be used.

We conclude that an alignment concept for the full CMS tracker is available, which meets the requirements. However, this is a study utilizing simulated data and real data will lead to further challenges. Systematic uncertainties, like the magnetic field uncertainty or thermal movements, are not yet included. However, the alignment strategy and the developed alignment tools are fully able to take these into account once they become available. On the other hand, data from beam halo muons and laser trajectories are expected to increase the sensitivity to poorly determined deformations, hence more emphasis can be given to the event data, making the survey measurements and the support structure information less important. Unfortunately, no simulated data for beam halo muons, the laser alignment system and survey measurements had been available. Minimum bias events and decay products of low mass resonances will have to be used as well in the early phase of data taking. The alignment strategy and tools described here can be used to align the CMS tracker with real data and can be extended to use more datasets than have been discussed here.

Acknowledgments

We would like to thank Volker Blobel for many helpful discussions and for making Millepede II available.

2008 JINST 3 P09002

References

[1] CMS collaboration, *The CMS tracker system project technical design report*, CERN-LHCC-98-006 CMS-TDR-005.

[2] CMS collaboration, *Addendum to the CMS Tracker TDR by the CMS collaboration*, CERN-LHCC-2000-016 CMS-TDR-005-add-1.

[3] A. Ostaptchouk et al., *The alignment system of the CMS tracker*, CMS-NOTE-2001-053.

[4] V. Blobel and C. Kleinwort, *A new method for high-precision alignment of track detectors*, contribution to the *Conference on Advanced Statistical Techniques in Particle Physics*, Durham U.K., March 18–22 (2002), [hep-ex/0208021].

[5] V. Blobel, *Millepede II manual DRAFT*, http://www.desy.de/∼blobel (2007).

[6] V. Blobel and E. Lohrmann, *Statistische und Numerische Methoden der Datenanalyse*, Teubner (1998) [ISBN: 3-519-03242-0].

[7] M. Stoye, *Calibration and alignment of the CMS silicon tracker*, PhD thesis, University of Hamburg, July (2007), CERN-THESIS-2007-026.

[8] R. Barrett et al. *Templates for the solution of linear systems: building blocks for iterative methods*, SIAM, 2nd Edition, (1994).

[9] C.C. Paige and M.A. Saunders, *Solution of sparse indefinite systems of linear equations*, *SIAM J. Numer. Anal.* **12** (1975) 617.

[10] G.H. Golub and C.F. Van Loan, *Matrix computations* 3rd ed., section 4.2, Johns Hopkins University Press (1996) [ISBN: 0-8018-5414-8].

[11] T. Sjöstrand et al., *High-energy-physics event generation with PYTHIA 6.1*, *Comput. Phys. Commun.* **135** (2001) 238.

[12] I. Belotelov et al., *Simulation of misalignment scenarios for CMS tracking devices*, CMS-NOTE-2006-008.

[13] CMS collaboration,*CMS physics: Technical Design Report Vol 1. Detector performance and software*, CERN-LHCC-2006-001, CMS-TDR-008-1.

[14] E. Widl et al., *Representation and estimation of trajectories from two-body decays*, CMS-NOTE-2007-032.

2008 JINST 3 P09002